Theoretical Examination of the Global Fluid Phase Behavior and Critical Phenomena in Carbon Dioxide + *n*-Alkane Binary Mixtures

Amparo Galindo[†] and Felipe J. Blas*[,†,‡]

Department of Chemical Engineering and Chemical Technology, Imperial College of Science, Technology and Medicine, Prince Consort Road, London SW7 2BY, U.K., and Departamento de Física Aplicada, Escuela Politécnica Superior, Universidad de Huelva, 21819 La Rábida, Huelva, Spain

The phase behavior of carbon dioxide + *n*-alkane binary mixtures is studied using the statistical associating fluid theory for potentials of variable attractive range. Extensive experimental data is available in the literature concerning the homologous series of carbon dioxide + *n*-alkane systems; these provide an excellent example of the continuity of fluid phase behavior in binary mixtures. Continuous transitions in the types of phase behavior are observed as the molecular weight of the *n*-alkane is increased. In our work, the carbon dioxide and *n*-alkane molecules are treated as attractive spherical segments tangentially bonded together. The attractive interactions are included as square-well potentials of depth ϵ and range λ. The pure component parameters of carbon dioxide are obtained by fitting to experimental vapor pressure and saturated liquid density data from the triple to the critical point, and the optimized molecular parameters of *n*-alkanes are taken from a set of transferable parameters previously presented [McCabe and Jackson, *Phys. Chem. Chem. Phys.* **1999**, *1*, 2057]. The optimized conformal molecular parameters (segment size and dispersive energy) are rescaled in order to give the best description of the experimental critical points. The critical lines and critical end-points, which determine the types of phase behavior, are predicted by the SAFT-VR approach in very good agreement with experimental data. This is particularly gratifying as the unlike dispersion interaction and range of the potential between carbon dioxide and alkane segments are obtained from a single mixture (CO_2 + *n*-tridecane) and then transferred to the other systems.

1. Introduction

Supercritical carbon dioxide (CO_2) is a useful and benign replacement for many organic solvents used in the traditional chemistry and oil industries. It is often considered as an ideal substitute to the standard organic solvents because it is nonflammable, essentially nontoxic, and the least expensive solvent after water. It has a critical temperature near ambient temperature (T_c = 304.21 K,[1] as compared to the critical temperature of water which is 647 K[2]), a reasonable critical pressure (P_c = 7.383 MPa,[1] whereas that of water is 22 MPa approximately[2]), and a critical density higher than that of most other supercritical solvents. Carbon dioxide has no dipole moment because of its molecular symmetry, but it presents a significant quadrupole moment. It is, however, a low dielectric-constant fluid, and consequently, a relatively poor solvent of many polar and organic compounds, including long-chain *n*-alkanes, water, polymers, and in general hydrophilic compounds. One of the most successful strategies to overcome this limitation has been to make use of CO_2-philic functional groups in order to increase the solubility of the molecules in CO_2. Experimental results show that fluorinated alkanes, ethers, and polymers are much more soluble in CO_2 than their hydrocarbon counterparts,[3−5] but there is considerable controversy over the origin of this high solubility (for more details see the work of Diep et al.[6] and references therein).

Mixtures of carbon dioxide + *n*-alkanes have been measured extensively, and there is a vast amount of reliable experimental phase equilibria and critical data. From a theoretical point of view, the homologous series of CO_2 + *n*-alkane binary mixtures provides an excellent opportunity to confirm the continuity in fluid phase behavior that can be observed in mixtures as an extension of the continuous gas−liquid critical transition that exists in pure fluids (see ref 7 and references therein). Scott and van Konynenburg[2,8,9] used the van der Waals equation of state to study binary fluid phase behavior, classifying the mixtures by the topology of the critical lines, and were able to present a global phase diagram indicating the continuous transitions between the different types of phase behavior. In their scheme, five of the six types of known binary phase behaviors were presented. Four of these are relevant to mixtures of carbon dioxide + *n*-alkanes. In type I systems, the two components are of similar nature, the mixture exhibits a continuous gas−liquid critical line connecting the critical points of the two pure components, whereas no liquid−liquid separation is seen. As the two components become more dissimilar, liquid−liquid separation can be observed if the solid phases are present at low enough temperatures. These are so-called type II mixtures. Together with a continuous gas−liquid critical curve, a second liquid−liquid critical line, which denotes the boundary of liquid−liquid immiscibility, extends from an upper critical end point (UCEP) (the limit of gas−liquid-liquid coexistence) to high pressures. In the low-pressure region of the phase diagram, the liquid−liquid−vapor three-phase line continues from the UCEP to low temperatures and pressures. Type III systems are characterized by extensive liquid−liquid immiscibility. In these systems, the liquid−liquid−vapor three-phase line extends from low pressures and temperatures to an UCEP found close to the critical point of the more volatile component. A short gas−liquid critical line is seen between the UCEP and the gas−liquid critical point of the volatile component. A second fluid−fluid

* To whom all correspondence should be addressed. E-mail: Felipe.Jimenez@dfaie.uhu.es. Fax: +34 959 017304.
† Imperial College of Science, Technology and Medicine.
‡ Universidad de Huelva.

10.1021/jp013402h CCC: $22.00
Published on Web 04/05/2002

critical line starts from the gas−liquid critical point of the less volatile component continuing to high pressures. Type IV phase behavior corresponds to the transition between types II and III. In type IV phase behavior, the system exhibits two immiscible liquid phases at low temperatures with a liquid−liquid−vapor three-phase line starting at very low temperatures and pressures and finishing at an UCEP as seen in systems exhibiting type II phase behavior. However, close to the critical point of the more volatile component, a second region of immiscibility is found which is bound below by a lower critical end point (LCEP) and above by a second UCEP. As a result, the gas−liquid critical line is discontinuous in these systems, with a first part extending from the critical point of the less volatile component to the LCEP and a second one extending from the second UCEP to the critical point of the more volatile component.

The experimental data of carbon dioxide + *n*-alkane mixtures are central to this study; hence, it is important to acknowledge a number of studies that have been undertaken for these systems; a brief overview of the available data is presented before details of the theoretical approach are discussed. The first published work regarding the investigation of the phase behavior of binary carbon dioxide + hydrocarbon mixtures is perhaps due to Kuenen and co-workers in 1897[10,11] and 1902,[12] who studied mixtures of carbon dioxide + ethane ($CO_2 + C_2H_6$). Extensive experimental data involving mixtures of carbon dioxide with small alkanes (up to *n*-pentane) can be found in references.[13−32] The phase behavior of carbon dioxide mixtures with heavier hydrocarbons was studied during the 1950s and the 1960s,[33−42] including mixtures of carbon dioxide with *n*-alkanes up to *n*-tetratetracontane (n-$C_{44}H_{90}$). Of special relevance to our present study is the pioneering experimental work of Schneider and co-workers,[43−46] who showed that the carbon dioxide + *n*-alkane homologous binary mixtures exhibit types of phase behavior which can be easily and gradually varied over wide ranges of conditions by increasing the molecular weight of the alkane chain. In this way, they confirmed that in the mixtures continuous transitions between gas−liquid, liquid−liquid, and gas−gas equilibria occur. They measured the critical behavior for a number of mixtures from the quadruple or solid−liquid−liquid−vapor (SLLV) point to the critical point, for pressures up to 1500 bar (150 MPa). Type II phase behavior was observed for CO_2 + n-C_8H_{18} and CO_2 + *n*-undecane (n-$C_{11}H_{24}$), whereas it was suggested that CO_2 + *n*-tridecane (n-$C_{13}H_{28}$) belongs to a transition type, and the mixture of CO_2 + n-$C_{16}H_{34}$ exhibits type III phase behavior. Sometime later Kulkarni et al.[47] confirmed that the phase behavior of CO_2 + n-$C_{10}H_{22}$ can be classified as type II phase behavior. More recently, van der Steen et al.[48] have confirmed the previous results of Schneider and co-workers and measured the liquid−liquid−vapor equilibria of the CO_2 + *n*-tetradecane (n-$C_{14}H_{30}$), + *n*-pentadecane (n-$C_{15}H_{32}$), and + n-$C_{16}H_{34}$ binary mixtures, which clearly suggests that the mixtures exhibit type III phase behavior.

Hottovy et al.[49] measured the phase behavior of carbon dioxide + n-$C_{13}H_{28}$ but concluded that the mixture exhibits type II phase behavior. Enick et al.[50] and Fall and Lucks,[51] motivated by the controversial results of Schneider and co-workers and Hottovy et al., have reexamined the phase behavior of CO_2 + n-$C_{13}H_{28}$. They have independently shown that this system is characterized by two liquid−liquid−vapor loci and a discontinuous gas−liquid critical curve; that is, this mixture exhibits type IV phase behavior, as corresponds to the transition between types II and III.

It is also of interest to consider which is the smallest alkane to exhibit limited solubility in carbon dioxide. In the 1970s, Jensen,[52] Im,[53] and Francis[54] showed that a definite tendency toward partial miscibility exists in the mixtures of carbon dioxide with heavy hydrocarbons. Im and Kurata[55] measured the phase behavior of carbon dioxide in *n*-hexane and *n*-heptane from 216.56 K up to the eutectic point of the mixtures. These authors have found that both systems exhibit partial miscibility in the upper range of the solubility curve, but the immiscibility gap turns out to be metastable in the CO_2 + n-C_6H_{14} (it appears at 213.7 K, i.e., below the solidification line), whereas in the CO_2 + n-C_7H_{16} mixture, the immiscibility gap is stable and extends approximately 7 K above the normal solubility curve. When the classification of Scott and Konynenburg is followed, the CO_2 + n-C_6H_{14} mixture exhibits type I phase behavior (miscible liquid phase), whereas the CO_2 + n-C_7H_{16} mixture belongs to type II (immiscible liquid phase). Miller and Lucks[56] studied the topography of the phase diagrams of carbon dioxide + *n*-alkane in order to estimate the immiscibility limits for the homologous series of binary mixtures. The paper contains an excellent review of most of the works on heterogeneous phase behavior of these systems, looking in particular at the critical end-points of CO_2 + n-C_7H_{16};[55] + n-C_8H_{18};[57] + n-$C_{10}H_{22}$;[47] + *n*-dodecane (n-$C_{12}H_{26}$);[49] + n-$C_{13}H_{28}$;[49,51] and + n-$C_{14}H_{30}$ and + n-$C_{15}H_{32}$;[49] + *n*-nonadecane (n-$C_{19}H_{40}$);[58] + n-$C_{20}H_{42}$;[39,58] and + *n*-heneicosane (n-$C_{21}H_{44}$).[58]

To recap, mixtures of carbon dioxide with *n*-alkanes shorter than, and up to, *n*-hexane exhibit type I phase behavior. Mixtures of carbon dioxide with *n*-alkanes from *n*-heptane up to *n*-dodecane are seen to exhibit phase behavior of type II. The mixture of carbon dioxide + *n*-tridecane corresponds to type IV, whereas mixtures of carbon dioxide with *n*-tetradecane, and with longer *n*-alkanes, exhibit type III phase behavior because of the increased immiscibility between the two components. The transition in phase behavior from type II through type IV into type III presents two interesting border-line cases: type II/IV and type IV/III. The first case is characterized by the presence of a tricritical point on the uninterrupted gas−liquid critical line; increased immiscibility in the system results in the two critical end points characteristic of type IV mixtures. In the IV/III transition, a double-critical point can be seen on the liquid−liquid−vapor three-phase line. At the double critical point, the gas−liquid and liquid−liquid critical curves merge into a single critical curve characteristic of type III phase behavior. It should be mentioned that these transitions are also observed in other homologous series of mixtures.[59] In a theoretical study, such as the one of Scott and van Konynenbug and such as the one presented here, the intermolecular parameters can be changed continuously, so that the transition phase diagrams and tricritical and double-critical points can always be obtained. In experimental systems, however, only occasionally do these delicate transitions occur for compounds which are available. Often pseudo-binary systems have been used in order to observe this behavior.[2]

To predict the thermodynamic properties of carbon dioxide + *n*-alkanes, two important features must be included at an early stage of a theoretical description, namely, the nonspherical (chainlike) nature of both the *n*-alkane and the carbon dioxide molecules, and the electrostatic interactions due to the quadrupole moment of CO_2. Both of these features cause anisotropies in the molecular interactions and are responsible for large nonidealities in the mixtures. Traditional theoretical approaches, including activity coefficient models and the so-called cubic equations of state, are commonly used to correlate this kind of systems, although they rarely incorporate anisotropic interactions. The Wilson, NRTL, and UNIQUAC equations[60] have

been used with relative success. Cubic equations of state, such as the Peng−Robinson[61] or the Soave−Redlich−Kwong (SRK)[62] equations, are also extensively used in the study of systems formed by chain molecules even though they do not explicitly account for nonsphericity. In particular, Coutinho et al.[63] have applied the SRK equation of state to determine the phase behavior of CO_2 + *n*-alkane binary mixtures. These approaches provide powerful correlation tools, but their applicability is usually limited to the specific systems and conditions of the correlation, in this sense having little predictive value.

Recently, more rigorous approaches are based on a knowledge of the intermolecular interaction forces between the molecules that form the system. The interactions are defined in terms of molecular parameters with physical meaning, which are state-independent. These are usually approaches with wider predictive capabilities. In particular, a number of these explicitly account also for the nonspherical shape of molecules. Beret and Prausnitz[64] developed the perturbed hard chain theory (PHCT) in order to include molecular motions because of rotational and vibrational degrees of freedom of the chain. The original PHCT, however, contains a rather cumbersome representation of the attractive interactions derived from a perturbation expansion for square-well molecules. Kim et al.[65] introduced the simpler attractive term of Lee et al.[66] in the development of the simplified perturbed hard chain theory (SPHCT).

Whereas there have been a large number of works dealing with nonspherical molecules, less common are the approaches developed specifically to take into account electrostatic interactions. In a pioneering work, Twu and Gubbins[67,68] developed a theory for the thermodynamic properties of polyatomic fluid mixtures which explicitly accounts for electrostatic intermolecular forces (dipole, quadrupole, etc.) as well as for the anisotropic charge overlap (shape) forces. The theory, based on a multipole series which uses the Padé approximant introduced by Stell et al.,[69] describes accurately the vapor−liquid equilibria of pure and fluid mixtures composed by polar, quadrupolar, and octopolar small and nearly-spherical molecules. The PHCT and SPHCT approaches have been extended, using the expansion of Twu and Gubbins, to describe anisotropic multipolar interactions.[70] More recently, Benavides et al.[71−73] have developed a new perturbation theory for polar fluids, in which the overlap and dispersion forces are taken into account through the square-well potential, and the electrostatic interactions arising from forces between point multipoles are described through a Padé approximation similar to that used by Twu and Gubbins.[67,68] They have used this approach to predict the thermodynamic properties (vapor pressures, coexistence diagrams, speed of sound, and molar isochoric heat capacities) of carbon dioxide and nitrogen, finding an excellent agreement with experimental data.[74]

The statistical associating fluid theory (SAFT)[75,76] is also a molecular-based equation of state, which stems from Wertheim's first-order thermodynamic perturbation theory for associating[77−80] and chain molecules.[81−84] The SAFT approach has since been used to study the phase equilibria of a wide variety of pure components and their mixtures, and it is now considered one of the most reliable predictive tools for the study of fluid phase equilibria. At the same time, many modifications following the general SAFT framework have also been presented. In general, it combines a chain reference contribution with an associating perturbation term for the description of complex chain and associating fluids. Huang and Radosz were the first to use a variation of the approach to successfully correlate the phase behavior of a large number of pure fluids and mixtures.[85,86] We recommend the excellent reviews in refs 87 and 88 for more details. Here, we give only a brief account of some of most commonly used versions of the approach and some recent new developments.

In the simplest SAFT-HS theory,[81,82] the molecules are modeled as chains of hard-sphere segments tangentially bonded with attractive dispersion interactions described at the mean-field level of van der Waals. This equation has been successfully applied to predict the phase equilibria of systems in which one or two components are strongly associated,[89−92] and it has been extended to take into account branched chain fluids[93] using the first- and second-order thermodynamic perturbation theory of Wertheim. However, this approach is in general not adequate for systems where the dispersive interactions play a dominant role, such as alkane fluids. In the SAFT-VR model,[94,95] chains of attractive segments (usually, although not necessarily, square-well segments[96,97]) are considered. The advantage of SAFT-VR over other versions of SAFT is that it allows the treatment of nonconformal properties, such as electrostatic interactions, of the fluid under consideration. It has been used to accurately model the phase behavior of a number of fluids and mixtures,[98−103] and it has been extended to study electrolyte[104,105] and polymer fluids.[106] Sadowski and co-workers[107,108] have developed the so-called perturbed-chain SAFT by applying the perturbation theory of Barker and Henderson with a hard-chain reference fluid, instead of the usual monomer reference system. The theory, which is in good agreement with simulation data of square-well chains,[107] is found to give an accurate description of the phase equilibria of a wide number of real substances and their mixtures.[108]

Associating chains of Lennard-Jones segments have also been studied by a number of authors.[109−114] In particular, Müller and Gubbins[115] and Kraska and Gubbins[116,117] have extended the SAFT approach for Lennard-Jones systems including a Helmholtz free energy contribution due to electrostatic interactions. Similarly, Jog and Chapman[118] incorporated the multipolar expansion of Twu and Gubbins to study dipolar chains formed by hard spherical segments. A recent version of SAFT for Lennard-Jones molecules, the so-called *Soft*-SAFT equation of state, has been extended to deal with mixtures of homonuclear and heteronuclear Lennard-Jones chains.[119] This theory has proved to be very accurate in predicting the thermodynamic properties and phase equilibria behavior of model and real hydrocarbons mixtures,[119−122] and (based on the work of Johnson[123]) it has been extended to account for the formation of mixtures of Lennard-Jones chains using a dimer reference fluid.[124] More recently, Pàmies and Vega[125] have proposed a new set of transferable parameters for the *Soft*-SAFT equation of state to predict the phase equilibria of the *n*-alkanes and their mixtures.

New developments related to the formalism of Wertheim include the work of Vega and MacDowell,[126] in which solid phases of hard-sphere chain molecules are considered, and a study of the vapor−liquid interface and surface tension of associating and chain fluids determined using a local density functional theory (DFT) that reduces to the SAFT-HS Helmholtz free energy in the bulk limit.[127,128] Several authors have also applied the SAFT equation of state to study other thermodynamic properties such as excess functions.[129−132]

Although the SAFT approach has been used to predict the phase behavior of a large number of model and real systems, only a few studies have concentrated in mixtures containing carbon dioxide. Using the original version of the approach, Huang and Radosz[85,86] have correlated the molecular parameters

of pure CO_2 and studied the CO_2 + *n*-$C_{10}H_{22}$ mixture. Passarello et al.[133] have carried out a comprehensive study of the mutual solubilities of carbon dioxide and alkanes, considering linear alkanes from C_3H_8 to *n*-$C_{44}H_{90}$ and branched alkanes. They chose a transferable approach of the intermolecular interaction parameters in order to predict the solubilities in the mixtures. They obtain reasonable agreement with the experimental data in most cases. In this extensive work, unfortunately, only vapor−liquid equilibria are considered and the global phase behavior is not presented. Mixtures of supercritical carbon dioxide with polymers[134,135] and organic acids[136] have also been studied with different versions of the SAFT approach.

Molecular simulations can provide exact calculations relating the intermolecular parameters to phase equilibria. Especially relevant to our work is the study of Potoff et al.,[137] who have obtained the phase behavior of carbon dioxide + *n*-alkane mixtures using grand canonical histogram-reweighting Monte Carlo simulations. Two combining rules for the intermolecular parameters are considered. The main conclusion seems to be that the Lorentz−Berthelot combining rule is not adequate for describing these complex mixtures, but it is difficult to translate the values of the unlike intermolecular parameters to those in our SAFT approach. More recently, Potoff and Siepmann[138] have presented a new force field for CO_2 and studied the vapor−liquid equilibria of carbon dioxide + propane and + *n*-hexane binary mixtures using the Lorentz−Berthelot combining rules. Agreement between experimental data and simulation results is excellent in all cases. Cui et al.[139] have also studied the vapor−liquid behavior of carbon dioxide + *n*-alkane and + perfluoro-*n*-alkane binary mixtures using the Gibbs ensemble Monte Carlo simulation technique. Perfluoroalkane molecules are considerably more soluble in CO_2 than their alkane counterparts, an important fact in terms of the supercritical extraction of organic substances in CO_2; the cause of the different solubility is not yet fully understood.

In this work, we aim at obtaining a picture of the global phase behavior of carbon dioxide + *n*-alkane mixtures. We have already presented a preliminary study in which it was shown that, using the SAFT-VR approach with two adjusted transferable parameters, the delicate transition between phase behavior of types II, IV, and III can be obtained.[140] Now a more extensive range of mixtures of carbon dioxide with *n*-alkanes, from ethane to *n*-hexadecane, is studied in detail, and we concentrate on the transitions in the type of phase behavior following the classification of Scott and van Konynenburg. In the future, we plan to extend the approach to study the solubility of polymers in supercritical CO_2. Furthermore, the SAFT-VR approach has also been used to study mixtures of alkane and perfluoroalkane molecules.[100] Alkane + perfluoroalkane mixtures exhibit a marked immiscibility in the liquid phase, indicating the different nature in the interactions and geometric packing between the two compounds. We hope to be able to combine the knowledge of the intermolecular parameters in these mixtures to compare the solubilities of alkanes and perfluoroalkanes in carbon dioxide. The rest of the paper is organized as follows: in section 2, we present the most relevant features of the molecular model and the SAFT-VR equation of state, results and discussion are presented in section 3, and conclusions are presented in section 4.

2. Molecular Model and Theory

As in earlier work,[87,88,141] the alkane molecules are modeled with a simple united atom approach, in which *m* hard-sphere attractive segments of equal diameter σ are bonded tangentially to form chains. The united atom model takes into account the main attributes of chain molecular architecture, i.e., bead connectivity, to represent topological constrains and internal flexibility, excluded volume effects, and attractions between the different beads that form the chains (inter- and intramolecular dispersion interactions are taken into account). Although it should be noted that some of the finer details of the chain conformation, such as flexibility and branching, are not incorporated; in particular, the anomalous critical pressure of methane cannot be predicted in a united atom approach. In the SAFT-VR version of the approach, the attractive interactions between two segments *i* and *j* are usually described via a square-well potential. The approach is, however, entirely general, and other attractive potentials can be used. The square-well potential is given by

$$u_{ij}(r) = \begin{cases} +\infty & \text{if } r < \sigma_{ij} \\ -\epsilon_{ij} & \text{if } \sigma_{ij} \le r < \lambda_{ij}\sigma_{ij} \\ 0 & \text{if } r > \lambda_{ij}\sigma_{ij} \end{cases} \quad (1)$$

where *r* is the distance between the two segments, σ_{ij} defines the contact distance between spheres, and λ_{ij} and ϵ_{ij} are the range and depth of the potential well for the *i*−*j* interaction, respectively.

The SAFT-VR approach has already been presented.[94,95] Here, we only give an overview of the main expressions. The equation is written in terms of the Helmholtz free energy. In the case of nonassociating molecules, the free energy can be expressed as a sum of three microscopic contributions: an ideal contribution A^{IDEAL}, a monomer term A^{MONO}, which takes into account the attractive and repulsive forces between the segments that form the molecules, and a chain contribution A^{CHAIN}, which accounts for the connectivity of the molecules. The free energy is then written as

$$\frac{A}{Nk_BT} = \frac{A^{\text{IDEAL}}}{Nk_BT} + \frac{A^{\text{MONO}}}{Nk_BT} + \frac{A^{\text{CHAIN}}}{Nk_BT} \quad (2)$$

where *N* is the total number of molecules, *T* is the temperature, and k_B is the Boltzmann constant.

2.1. The Ideal Mixture. The free energy of the ideal mixture is given by[142]

$$\frac{A^{\text{IDEAL}}}{Nk_BT} = \sum_{i=1}^{n} x_i \ln(\rho_i \Lambda^3_i) - 1 \quad (3)$$

where $\rho_i = N_i/V$ is the number density and Λ_i is the thermal de Broglie wavelength of species *i*.

2.2. The Monomer Contribution. The monomer free energy can be written as

$$\frac{A^{\text{MONO}}}{Nk_BT} = (\sum_{i=1}^{n} m_i x_i) a^{\text{M}} \quad (4)$$

where m_i is the number of spherical segments in each chain *i*. The excess monomer free energy per segment of the mixture, $a^{\text{M}} = A^{\text{MONO}}/(N_s k_B T)$, where N_s is the total number of spherical segments, is obtained from the high-temperature expansion of Barker and Henderson[143−145]

$$a^{\text{M}} = a^{\text{HS}} + \frac{1}{k_BT} a_1 + \frac{1}{(k_BT)^2} a_2 \quad (5)$$

where a^{HS} is the excess free energy per segment in a mixture of hard spheres and a_1 and a_2 are the first- and second-order perturbation terms associated with the attractive interactions $u_{ij}(r)$ given by eq 1.

$$a^{HS} = \frac{6}{\pi\rho_s}\left[\left(\frac{\zeta_2^{\,3}}{\zeta_3^{\,2}} - \zeta_0\right)\ln(1-\zeta_3) + \frac{3\zeta_1\zeta_2}{1-\zeta_3} + \frac{\zeta_2^{\,3}}{\zeta_3(1\text{-}\zeta_3)^2}\right] \quad (6)$$

where the number density of spherical segments in the mixture, $\rho_s = N_s/V$, is related to the total number density of molecules ρ, through the relationship

$$\rho_s = (\sum_{i=1}^{n} m_i x_i)\rho \quad (7)$$

The reduced densities ζ_l are defined as

$$\zeta_l = \pi/6\rho_s[\sum_{i=1}^{n} x_{s,i}\sigma_{ii}^{\,l}] \quad (8)$$

where σ_{ii} is the diameter of the spherical segments in chain i and $x_{s,i}$ is the mole fraction of segments of type i in the mixture, given by

$$x_{s,i} = \frac{m_i x_i}{\sum_{j=1}^{n} m_j x_j} \quad (9)$$

The overall packing fraction of the mixture is thus given by ζ_3, which is equivalent to η, the packing fraction in the pure component case.

The mean-attractive energy associated with the first-order perturbation term, a_1, is given by[94,95]

$$a_1 = \sum_{i=1}^{n}\sum_{j=1}^{n} x_{s,i}x_{s,j}a_1^{(ij)} \quad (10)$$

where

$$a_1^{(ij)} = -\rho_s\alpha_{ij}^{VDW}g_{ij}^{HS}[\sigma_{ij};\zeta_3^{eff}] \quad (11)$$

α_{ij}^{VDW} is the van der Waals attractive constant associated with the $i-j$ interaction

$$\alpha_{ij}^{VDW} = \frac{2\pi}{3}\epsilon_{ij}\sigma_{ij}^{\,3}(\lambda_{ij}^{\,3} - 1) \quad (12)$$

and $g_{ij}^{HS}[\sigma_{ij};\zeta_3^{eff}]$ is the contact pair distribution function of a mixture of hard spheres at density ζ_3^{eff}. In the van der Waals one (vdW-1) fluid theory, g_{ij}^{HS} is approximated by the contact pair distribution function of a pure hypothetical fluid with the molecular parameters defined by a set of mixing rules. This allows us to simplify eqs 10 and 11 to

$$a_1 = -\rho_s\sum_{i=1}^{n}\sum_{j=1}^{n} x_{s,i}x_{s,j}\alpha_{ij}^{VDW}g_0^{HS}[\sigma_m;\zeta_m^{eff}] \quad (13)$$

where g_0^{HS} is the contact value of the hard-sphere pair distribution function obtained from the Carnahan and Starling equation of state[148]

$$g_0^{HS}[\sigma_m;\zeta_m^{eff}] = \frac{1-\zeta_m^{eff}/2}{(1-\zeta_m^{eff})^3} \quad (14)$$

The effective packing fraction ζ_m^{eff} in eq 13 is obtained within the vdW-1 fluid approximation from the corresponding packing fraction of the mixture ζ_m

$$\zeta_m^{eff}(\zeta_m,\lambda_{ij}) = c_1(\lambda_{ij})\zeta_m + c_2(\lambda_{ij})\zeta_m^{\,2} + c_3(\lambda_{ij})\zeta_m^{\,3} \quad (15)$$

where

$$\zeta_m = \frac{\pi}{6}\rho_s\sum_{i=1}^{n}\sum_{j=1}^{n} x_{s,i}x_{s,j}\sigma_{ij}^{\,3} = \frac{\pi}{6}\rho_s\sigma_m^{\,3} \quad (16)$$

and

$$\sigma_m^{\,3} = \sum_{i=1}^{n}\sum_{j=1}^{n} x_{s,i}x_{s,j}\sigma_{ij}^{\,3} \quad (17)$$

The λ_{ij}-dependent coefficients, c_1, c_2, and c_3, are approximated by those of pure fluids, as in previous work[94,95]

$$\begin{pmatrix} c_1 \\ c_2 \\ c_3 \end{pmatrix} = \begin{pmatrix} 2.25855 & -1.50349 & 0.249434 \\ -0.669270 & 1.40049 & -0.827739 \\ 10.1576 & -15.0427 & 5.30827 \end{pmatrix}\begin{pmatrix} 1 \\ \lambda_{ij} \\ \lambda_{ij}^{\,2} \end{pmatrix} \quad (18)$$

The approximation corresponds to the MX1b mixing rule in reference.[95] We have chosen this mixing rule in order to be able to examine both the phase equilibria and critical points of the mixtures (see ref 95 for more details).

The second-order perturbation term a_2 is given by

$$a_2 = \sum_{i=1}^{n}\sum_{j=1}^{n} x_{s,i}x_{s,j}a_2^{(ij)} \quad (19)$$

The terms $a_2^{(ij)}$ are calculated using the local compressibility approximation, so that

$$a_2^{(ij)} = \frac{1}{2}K^{HS}\epsilon_{ij}\rho_s\frac{\partial a_1^{(ij)}}{\partial\rho_s} \quad (20)$$

where K^{HS} is the hard-sphere isothermal compressibility in the Percus−Yevick approximation

$$K^{HS} = \frac{\zeta_0(1-\zeta_3)^4}{\zeta_0(1-\zeta_3)^2 + 6\zeta_1\zeta_2(1-\zeta_3) + 9\zeta_2^{\,3}} \quad (21)$$

2.3. The Chain Contribution. In a mixture of chains formed by square-well segments, the chain contribution to the free energy can be written as[94,95,109]

$$\frac{A^{CHAIN}}{Nk_BT} = \sum_{i=1}^{n} x_i(1-m_i)\ln y_{ii}^{SW}(\sigma_{ii}) \quad (22)$$

where $y_{ii}^{SW}(\sigma_{ij}) = g_{ij}^{SW}(\sigma_{ij})\exp(-\beta\epsilon_{ij})$. The contact pair distribution function for a mixture of square-well molecules corresponding to the $i-j$ interaction can be obtained from a high-temperature expansion as

$$g_{ij}^{SW}(\sigma_{ij}) = g_{ij}^{HS}(\sigma_{ij}) + \frac{1}{k_BT}\epsilon_{ij}g_1(\sigma_{ij}) \quad (23)$$

TABLE 1: Optimized SAFT-VR Square-Well Intermolecular Potential Parameters[a]

substance	m	σ/Å	ϵ/k_B/(K)	λ	T_c^*	$P_c^* 10^3$	σ_c/Å	ϵ_c/k_B/(K)
CO_2	2.0	2.7864	179.27	1.5157	0.18146	5.15128	3.1364	168.89
C_2H_6	1.333	3.788	241.8	1.5326	0.16256	6.3708	4.0920	192.49
C_3H_8	1.667	3.873	261.9	1.5531	0.16442	5.4141	4.2249	204.87
n-C_4H_{10}	2.0	3.887	256.3	1.5675	0.17486	4.7585	4.3195	213.19
n-C_5H_{12}	2.333	3.931	265.0	1.5778	0.18403	4.2477	4.3921	217.99
n-C_8H_{18}	3.333	3.945	250.3	1.5959	0.20562	3.1883	4.5378	225.71
n-$C_{11}H_{24}$	4.333	3.973	259.7	1.6056	0.22107	2.5177	4.6036	230.12
n-$C_{13}H_{28}$	5.0	3.950	228.2	1.6098	0.22919	2.1932	4.6260	232.41
n-$C_{14}H_{30}$	5.333	3.961	251.9	1.6117	0.23276	2.0567	4.6340	233.41
n-$C_{16}H_{34}$	6.0	3.980	244.4	1.6145	0.23913	1.8233	4.6945	235.46

[a] m is the number of spherical segments in the model, σ is the hard-core diameter, and ϵ and λ are the depth and range of the square-well. The subscript c indicates that the parameters have been rescaled to the experimental critical point. $T_c^* = k_B T_c/\alpha$ and $P_c^* = Pb^2/\alpha$ are the reduced critical temperature and pressure, with $\alpha = 2\pi/3\sigma^3\epsilon(\lambda^3 - 1)$ and $b = \pi/6\sigma^3$.

The contact pair distribution function for the hard-sphere mixture, $g_{ij}^{HS}(\sigma_{ij})$, is given by the expression of Boublík[146]

$$g_{ij}^{HS}(\sigma_{ij};\zeta_3) = \frac{1}{1-\zeta_3} + 3\frac{D_{ij}\zeta_3}{(1-\zeta_3)^2} + 2\frac{(D_{ij}\zeta_3)^2}{(1-\zeta_3)^3} \quad (24)$$

with the parameter D_{ij} defined as

$$D_{ij} = \frac{\sigma_{ii}\sigma_{jj}}{\sigma_{ii}+\sigma_{jj}} \frac{\sum_{i=1}^{n} x_{s,i}\sigma_{ii}^2}{\sum_{i=1}^{n} x_{s,i}\sigma_{ii}^3} \quad (25)$$

The first-order perturbation term of the distribution function, $g_1(\sigma_{ij})$, can be obtained from a self-consistent method for the pressure using the Clausius virial theorem and the density derivative of the Helmholtz free energy, so that[94,95]

$$g_1(\sigma_{ij};\zeta_3) = g_0^{HS}[\sigma_{ij};\zeta_3] + (\lambda_{ij}^3 - 1)g_0^{HS}[\sigma_{ij};\zeta_3^{eff}]\zeta_3^{eff}\left(\frac{1}{3}\lambda_{ij}\frac{\partial\zeta_3^{eff}}{\partial\lambda_{ij}} - \zeta_3\frac{\partial\zeta_3^{eff}}{\partial\zeta_3}\right) \quad (26)$$

The chemical potential μ and compressibility factor Z can be easily obtained from the Helmholtz free energy using standard thermodynamic relations

$$\mu_i = \left(\frac{\partial A}{\partial N_i}\right)_{T,V,N_{j\neq i}} \quad (27)$$

and

$$Z = \frac{PV}{Nk_BT} = \sum_{i=1}^{n}\left(x_i - \frac{\mu_i}{k_BT}\right) - \frac{A}{Nk_BT} \quad (28)$$

These functions are required in order to determine the critical and phase behavior of the mixture. The gas−liquid and liquid−liquid critical lines are calculated by equating the second and third derivatives of the Gibbs free energy with respect to the mole fraction to zero. The phase equilibria between phases I and II in a mixture requires that the temperature, pressure, and chemical potential of each component in each phase be equal,[2] i.e.

$$T^I = T^{II}, \quad P^I = P^{II}, \quad \mu_i^I = \mu_i^{II} \quad (29)$$

The phase equilibria along the three-phase line in mixtures requires similar conditions given by[2]

$$T^I = T^{II} = T^{III}, \quad P^I = P^{II} = P^{III}, \quad \mu_i^I = \mu_i^{II} = \mu_i^{III} \quad (30)$$

The conditions for phase equilibria and for the critical points are solved numerically using a modified Marquart−Levenberg method.[149]

It is also useful to define a number of reduced parameters in the calculations. In a mixture, all of the parameters are reduced relative to one of the components, component 1 in our case, so that the reduced dimensionless temperatures and pressures are defined as $T^* = k_BTb_{11}/\alpha_{11}^{VDW}$ and $P^* = Pb_{11}^2/\alpha_{11}^{VDW}$, where the volume of a spherical segment is denoted by $b_{ii} = \pi\sigma_{ii}^3/6$ and a subscript c is sometimes used to denote the critical point.

3. Results

As mentioned earlier, in the homologous series of carbon dioxide + n-alkane mixtures, transitions in the type of phase behavior are observed for different chain lengths of the n-alkane molecules. Together with this, the solubility of n-alkanes and other organic molecules in carbon dioxide is important in the context of supercritical fluid extraction. We aim at understanding the transitions in the type of phase behavior of these systems, as well as in providing an approach to predict their phase behavior in good quantitative agreement with experimental data.

To be able to compare the calculations obtained from the theory with experimental data, we have optimized the pure component molecular parameters, σ, ϵ, m, and λ, using experimental vapor pressure and saturated liquid densities for each substance from the triple to the critical point. The optimized molecular parameters for carbon dioxide are shown in Table 1. As can be seen in Figure 1, the SAFT-VR approach with the optimized parameters gives a very good description of the vapor pressures and coexistence densities in the entire range of temperatures, with the exception of the critical region. This behavior is expected because SAFT-VR is a classical equation of state in which the density fluctuations that occur close to the critical point are not included. However, because we have an interest in the critical curves of the mixtures, we have rescaled the conformal parameters σ_{11} and ϵ_{11} to the experimental critical temperature and pressure. Although it is important to note the detriment in the calculated saturated liquid density because of the rescaling of the parameters, it will be clear at a later stage that a good description of the coexistence compositions and critical curves can be obtained with the re-scaled parameters.

Optimized parameter values for the n-alkane series have been obtained by McCabe and Jackson;[101] they also presented linear relationships for each of the intermolecular parameters σ, ϵ, and λ, as functions of the molecular weight. As in previous works,

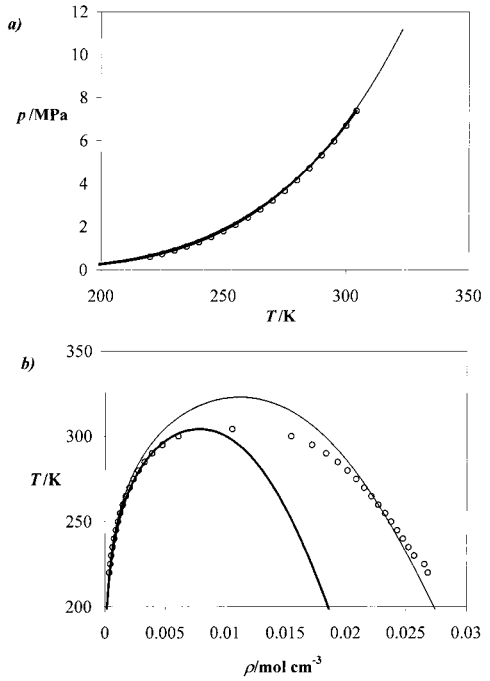

Figure 1. Carbon dioxide (a) vapor pressures and (b) coexistence densities. The circles represent the experimental data;[1] the thin curve corresponds to the SAFT-VR calculation with the optimized parameter values, and the bold curve corresponds to the theoretical results obtained using the molecular parameters rescaled to the critical point (see text and Table 1 for more details).

we use a simple empirical relationship to relate the number of carbon atoms in the *n*-alkane chain C and the number of spherical segments m_2 in the model: $m_2 = 1 + (C - 1)/3$. In the present work, we have used λ_{22} as obtained from the relationship $m_2\lambda_{22} = 0.03900M_{W2} + 0.873$,[101] where M_{W2} is the molecular weight of the *n*-alkane. As for carbon dioxide, the conformal parameters, σ_{22} and ϵ_{22}, are rescaled to the critical temperatures and pressures in order to obtain the best description of the critical region in each case (see Table 1).

The calculation of mixture phase equilibria also requires the determination of a number of cross or unlike parameters. The Lorentz combining rule is used for the unlike hard-core diameter

$$\sigma_{12} = \frac{\sigma_{11} + \sigma_{22}}{2} \tag{31}$$

whereas the unlike dispersive energy of the system is defined as

$$\epsilon_{12} = \xi(\epsilon_{11}\epsilon_{22})^{1/2} \tag{32}$$

where ξ describes the departure of the system from the Berthelot combining rule. A value of $\xi < 1$ is usually associated with liquid−liquid immiscibility. The unlike range parameter of the mixtures is obtained from the following equation:

$$\lambda_{12} = \gamma\frac{\lambda_{11}\sigma_{11} + \lambda_{22}\sigma_{22}}{\sigma_{11} + \sigma_{22}} \tag{33}$$

where γ is a second adjustable parameter which controls the range of the square-well interactions between carbon dioxide and *n*-alkane segments.

As discussed in the Introduction, carbon dioxide + *n*-alkane binary mixtures exhibit different phase behavior depending the length of the *n*-alkane chain. The transition from type II to type III through type IV phase behavior is one of the most delicate phenomena observed in these systems, as only one of the homologous mixtures (CO_2 + *n*-tridecane) corresponds to the intermediate type IV phase behavior.[50,51,56] The two unlike adjustable parameters ξ and γ were determined ensuring that this transition in phase behavior is observed: the optimized values are $\xi = 0.88$ and $\gamma = 0.989$. The unlike parameters can then be used in a transferable manner to predict the phase behavior of a number of carbon dioxide + *n*-alkane mixtures. Using the optimized parameters, the *PTx* phase diagram of CO_2 + *n*-$C_{13}H_{28}$ is calculated (a *PT* projection is shown in Figure 2). As can be seen, the SAFT-VR equation of state predicts type IV phase behavior for the mixture, in agreement with the experimental data of Enick et al.[50] and Fall and Luks.[51,56] See also Table 2 and the inset of Figure 2 and Figure 9. In the comparison of the experimental data and the calculated results, it is clear that the SAFT-VR approach gives a good description of the phase behavior of the mixture, not only for the critical end-point loci but also for the critical lines on a wide range of

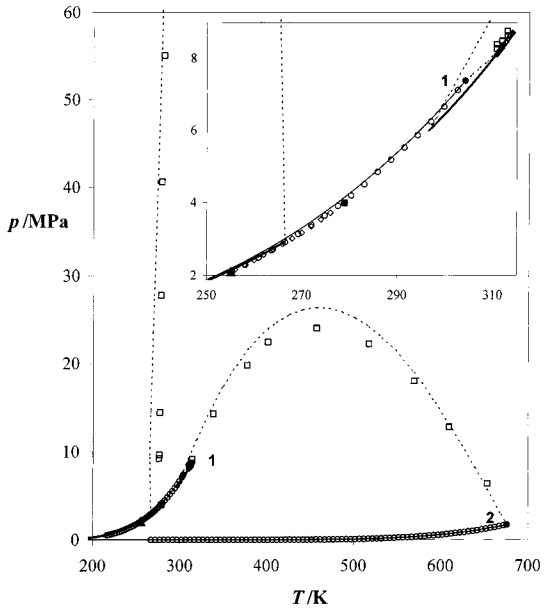

Figure 2. *PT* projection of the *PTx* surface for carbon a dioxide (1) + *n*-tridecane (2) mixture compared with the SAFT-VR calculations. The open circles represent the experimental pure component vapor pressures,[1,150] the filled circles the pure component critical points, the open squares the gas−liquid and liquid−liquid critical points,[45] the open diamonds the three-phase line,[50] the filled diamonds the LCEP and UCEPs,[49,51,56] and the filled triangle the SSLG quadrupole point.[49,56] The thin solid curves represent the calculated vapor pressures, the bold solid curves the predicted three-phase lines, and the dashed curves the calculated critical lines.

TABLE 2: Critical End-Point (CEP) Temperatures and Pressures for CO_2 + *n*-Alkane Mixtures[a]

n-alkane	type of CEP	T_{CEP}^{exp}/ K	T_{CEP}^{theory}/ K	P_{CEP}^{exp}/ MPa	P_{CEP}^{theory}/ MPa	ref
n-C_8H_{18}	UCEP[b]	231.49	241.29	0.922	1.379	56, 57
n-$C_{11}H_{24}$	UCEP[b]	256.63	253.71	2.110	2.040	45
n-$C_{12}H_{26}$	UCEP[b]	267.31	257.36	2.880	2.270	49, 56
n-$C_{13}H_{28}$	UCEP[b]	278.95	266.49	3.933	2.920	49, 51, 56
n-$C_{13}H_{28}$	LCEP	310.75	296.60	8.114	5.990	49, 51, 56
n-$C_{13}H_{28}$	UCEP[c]	314.01	312.12	8.716	8.420	49, 51, 56
n-$C_{14}H_{30}$	UCEP[c]	311.15	310.29	8.260	8.170	49

[a] The experimental and calculated values using the SAFT-VR approach are presented. [b] An upper critical end-point at low temperatures ($G + L_1 = L_2$). [c] An upper critical end-point at high temperatures ($L_2 + L_1 = G$).

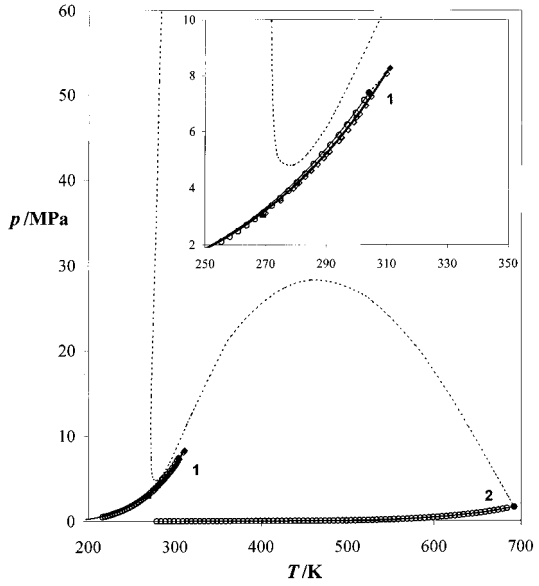

Figure 3. *PT* projection of the *PTx* surface for a carbon dioxide (1) + *n*-tetradecane (2) system compared with the SAFT-VR predictions. The open circles represent the experimental pure component vapor pressures,[1,150] the filled circles the pure component critical points, the open diamonds the three-phase line,[48,49] the filled diamond the UCEP,[49,56] and the filled triangle the SLLG quadrupole point.[49,56] The thin solid curves correspond to the calculated vapor pressures, the bold solid curve to the predicted three-phase line, and the dashed curves to the calculated critical lines.

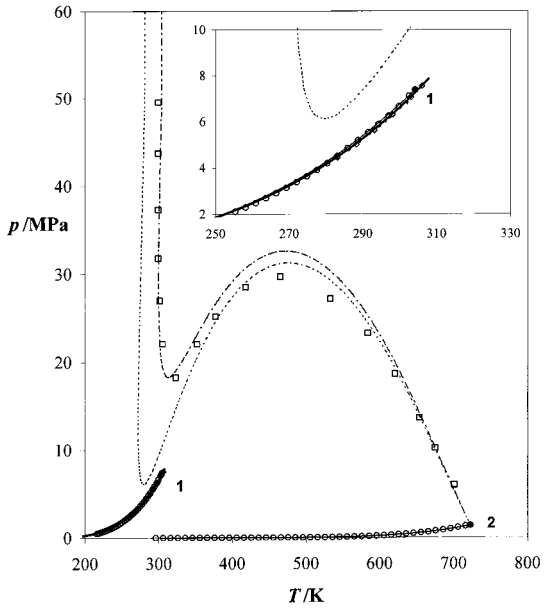

Figure 4. *PT* projection of the *PTx* surface for a carbon dioxide (1) + *n*-hexadecane (2) binary mixture compared with the SAFT-VR predictions. The open circles represent the experimental pure component vapor pressures,[1,150] the filled circles the pure component critical points, the open squares the gas−liquid and liquid−liquid critical points,[45] and the open diamonds the three-phase line.[48] The thin solid curves correspond to the calculated vapor pressures, the bold solid curve to the predicted three-phase line, and the dashed curves to the calculated critical lines using the transferable parameters ($\xi = 0.88$ and $\gamma = 0.989$). The long-dashed curve, corresponding to the fluid−fluid critical line, represents the theoretical results using $\xi = 0.8726$ and $\gamma = 0.989$.

thermodynamic conditions, including the high-pressure region of the phase diagram. It is important to note at this stage that the two adjusted unlike intermolecular parameters are state-independent.

As the chain length of the second component is increased, from *n*-tridecane to *n*-tetradecane, the immiscibility of the mixture also increases. The regions of three-phase coexistence, bounded by the critical end-points, are extended so that the high-temperature UCEP is seen to continue to slightly higher temperatures and pressures, whereas the UCEP at low temperatures merges with the LCEP. A unique three-phase line characteristic of type III phase behavior is observed. This transition from type IV to type III can be seen in Figure 3; the calculations using the SAFT-VR approach with two transferable parameters $\xi = 0.88$ and $\gamma = 0.989$ predict a phase diagram of type III for the mixture, in agreement with experimental data.[49,56] A continuous critical line, extending from the critical point of pure *n*-tetradecane to high pressures, exhibits a pressure maximum and minimum as the temperature is decreased. The calculated minimum in the critical line is so low that its *PT* projection appears to cut the vapor pressure curve of pure carbon dioxide (this is also observed experimentally[2]). The continuity of the vapor−liquid critical line, and of the three-phase line, is better seen in the inset of Figure 3. As can also be seen in the inset, the prediction of the UCEP is extremely good. See Table 2 for further details. The calculated data are, in this case, true predictions of the phase behavior of the CO_2 + *n*-$C_{14}H_{30}$ binary mixture; recall that the unlike intermolecular parameters were determined for the CO_2 + *n*-$C_{13}H_{28}$ mixture and have been transferred to model the phase behavior of this system.

If the number of carbon atoms of the *n*-alkane molecule is further increased, the increased immiscibility causes both the maximum and the minimum pressure found in the critical line to shift toward higher pressures and temperatures. In Figure 4, the results obtained from the SAFT-VR equation of state for the CO_2 + *n*-$C_{16}H_{34}$ system are shown. The predictions are in good qualitative agreement with the experimental data. The calculated phase diagram using the transferable parameters belongs to type III phase behavior, although deviations between the experimental data and the SAFT-VR predictions, especially in the region of high pressures, and close to the pressure minimum along the critical line of the system (see Figure 4) can be seen. Experimental results indicate that the critical line reaches its minimum at 323.15 K and 18.25 MPa and its maximum at 465.15 K and 29.68 MPa.[43−46] The calculated gas−liquid critical line with the transferable parameters exhibits a maximum in pressure at 471.5 K and 31.24 MPa and a LLG three-phase line (see the inset of Figure 4) in good agreement with experiments, but the minimum pressure in the critical line is predicted at 279.87 K and 6.13 MPa. Using a fully predictive approach, it is possible to obtain qualitative agreement with the experimental data for this system, and the correct type of phase behavior has been described with the calculations. Quantitative agreement can be obtained by slightly readjusting one of the unlike binary interaction parameters. The result of the calculations using $\xi = 0.8726$ (instead of $\xi = 0.88$) is shown in Figure 4. In the future, we plan to study the phase behavior of polymer molecules in carbon dioxide and can expect that the readjusted parameter may be more relevant for such systems.

The transferable approach can also be extended to *n*-alkane molecules shorter than *n*-tridecane. A mixture of CO_2 + *n*-$C_{12}H_{26}$ (see Figure 5) is found to exhibit type II/IV phase behavior. A continuous gas−liquid critical line is seen, but a slight change in the slope of the curve is observed close to the critical point of CO_2. We believe this corresponds to the onset of immiscibility in this region as is characteristic of mixtures of type IV. At low temperatures a region of liquid−liquid immiscibility is observed, and the UCEP predicted by the SAFT-

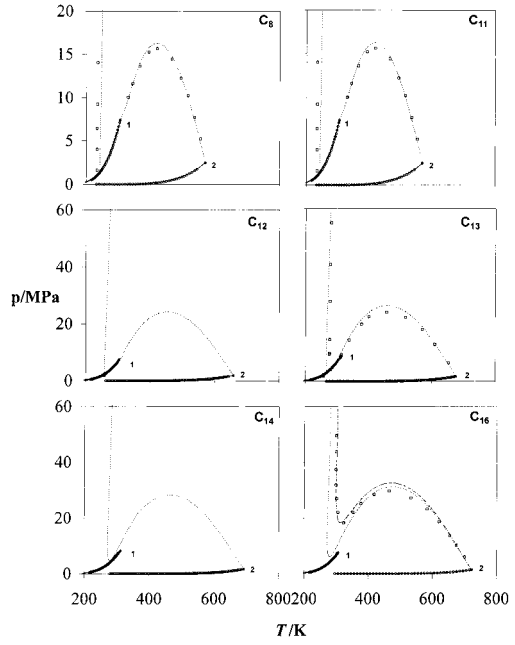

Figure 5. *PT* projections of the *PTx* surfaces for carbon dioxide (1) + *n*-alkane (2) systems compared with the SAFT-VR predictions. The symbols represent the experimental data, and the curves represent the SAFT-VR calculations. See Figures 2−4 for details.

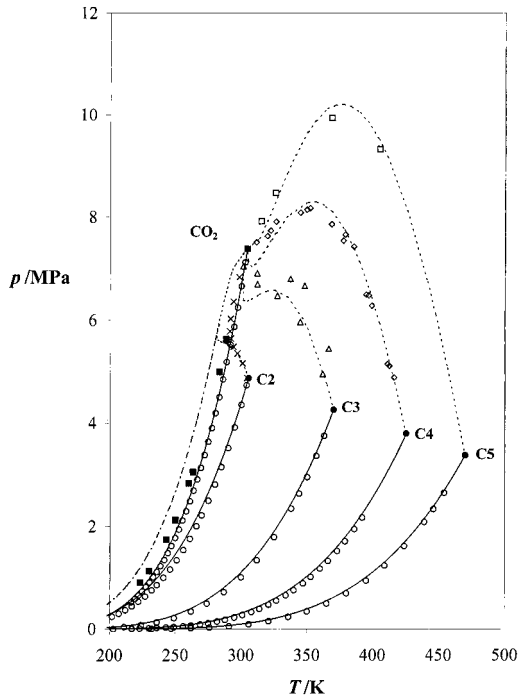

Figure 6. *PT* projection of the *PTx* surface for carbon dioxide(1) + ethane(2), + *n*-propane(2), + *n*-butane(2), and + *n*-pentane(2) binary mixtures compared with the SAFT-VR predictions. The open circles represent the experimental pure component vapor pressures,[1,150] the filled circles the pure component critical points, the open squares, open diamonds, open triangles and crosses the gas−liquid critical points of carbon dioxide + ethane,[23] + propane,[24,25,32] + *n*-butane,[24,25,32] and + *n*-pentane,[24] respectively, and the filled squares the azeotropic line of the carbon dioxide + ethane system.[11,13,15,17,19−22] The thin solid curves correspond to the calculated vapor pressures, the dashed curves to the predicted critical lines, and the dot−dashed curve to the calculated azeotropic curve corresponding to the carbon dioxide(1) + ethane(2) binary mixture.

VR calculation with $\xi = 0.88$ and $\gamma = 0.989$ is shown in Table 2 together with the experimental data. In the case of the CO_2 + *n*-$C_{11}H_{24}$ mixture (see Figure 5), the SAFT-VR approach is able to capture correctly the type II phase behavior exhibited by the mixture, providing an accurate description of both the gas−liquid and liquid−liquid critical lines as compared with experimental data. In this mixture, the critical locus of the UCSTs is seen at lower temperatures and extending to lower pressures than in the case of the CO_2 + *n*-$C_{12}H_{26}$ system. See Table 2 for further details.

A mixture of CO_2 + *n*-C_8H_{18} also exhibits type II phase behavior. The *PT* phase diagram corresponding to this mixture is shown in Figure 5, together with a number of the mixtures already presented. As can be seen, agreement between the experimental data and the theoretical predictions is excellent in a wide range of thermodynamic conditions; the locus of the gas−liquid critical line for the whole range of temperatures between the critical temperatures of both components, as well as the UCEP, are very well described by the calculations (see Table 2). The approach also provides a good description of the liquid−liquid critical line up to 50 MPa, although with a slight overestimation of the experimental values of Schneider and coworkers.[45]

It is useful to consider the transitions in phase behavior examining together a number of the mixtures already presented (see Figure 5). Type II phase behavior is observed for the CO_2 + *n*-C_8H_{18} and *n*-$C_{11}H_{24}$ systems. The CO_2 + *n*-$C_{12}H_{26}$ mixture is at the transition between types II and IV. We do not observe liquid−liquid separation in the critical region; it may not be present, or it may not be observable because of our numerical technique. A clear type IV phase behavior is observed for the CO_2 + *n*-$C_{13}H_{28}$ mixture. The mixtures with *n*-$C_{14}H_{30}$ and *n*-$C_{16}H_{34}$ exhibit type III phase behavior. It is important to emphasize that the binary interaction parameters ξ and γ have been chosen to ensure that the CO_2 + *n*-$C_{13}H_{28}$ binary mixture exhibits type IV phase behavior and have then been used to calculate the phase behavior of the other binary systems. As can be seen, using this set of transferable parameters, excellent agreement with the experimental critical data and three-phase behavior is obtained. More importantly, the continuous transitions in the types of phase behavior are also described by the theoretical approach.

The phase behavior of binary mixtures of carbon dioxide with shorter *n*-alkanes can also be examined using the same transferable parameters ($\xi = 0.88$ and $\gamma = 0.989$). In Figure 6, the *PT* projections of the *PTx* phase diagram corresponding to mixtures CO_2 + C_2H_6, + C_3H_8, + *n*-C_4H_{10}, and *n*-C_5H_{12}, are shown. Excellent agreement with experimental data is obtained in the prediction of the vapor−liquid critical curves characteristic of type I phase behavior.[13−31] It is interesting to note the change in curvature in the gas−liquid critical line of the CO_2+C_3H_8 mixture. This curvature is closely related with the fact that the CO_2 + C_2H_6 mixture exhibits minimum azeotropic behavior. Using the SAFT-VR approach with the transferable unlike parameters $\xi = 0.88$ and $\gamma = 0.989$, the phase behavior of the CO_2 + C_2H_6 can be predicted. The gas−liquid critical line, the presence of the azeotrope, and the existence of a minimum temperature in the critical locus are predicted by the approach (see Figures 6 and 7). However, some deviations between the experimental data and calculated results can be seen, especially for the azeotropic line and the critical points of the mixture close to the critical point of pure CO_2. It is of course possible to obtain quantitative agreement with the experimental data by readjusting the unlike interaction parameters. Although the set of transferable parameters gives a good description of the global phase behavior in the large homologous series studied (*n*-alkanes

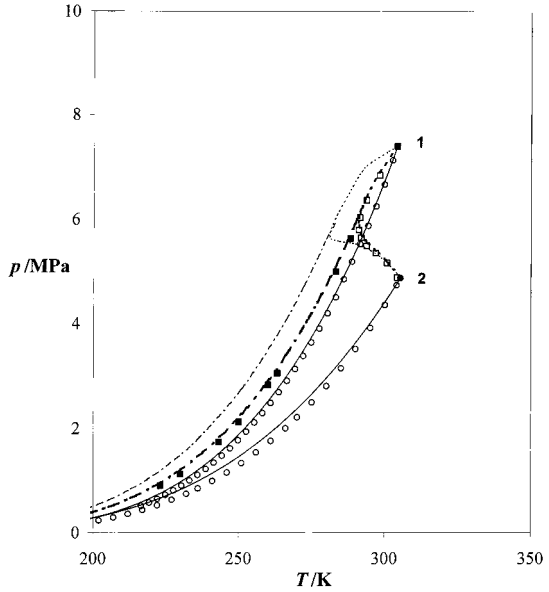

Figure 7. *PT* projection of the *PTx* surface for carbon dioxide (1) + ethane (2) mixture compared with the SAFT-VR predictions. The open circles represent the experimental pure component vapor pressures,[1,150] the filled circles the pure component critical points, the open squares the gas−liquid critical points,[23] and the filled squares the azeotropic line.[11,13,15,17,19−22] The thin solid curves correspond to the calculated vapor pressures, the thin dashed curve to the critical line, and the thin dot−dashed curve to the azeotropic curve using transferable parameters ($\xi = 0.88$ and $\gamma = 0.989$). The bold dashed curve and bold dot−dashed correspond to the critical and azeotropic curves, respectively, using $\xi = 0.94$ and $\gamma = 0.989$.

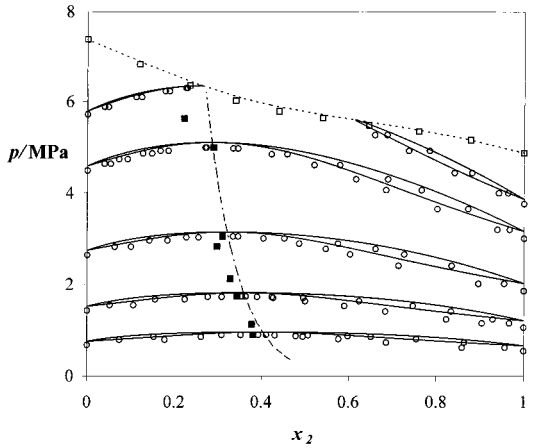

Figure 8. *Px* slices (starting at the lowest pressures) at 223.15, 243.15, 263.15, 283.15, and 293.15 K for carbon dioxide (1) + ethane (2) binary system compared with the SAFT-VR predictions. The symbols correspond to the experimental gas−liquid critical line (open squares),[23] the coexistence curves (open circles),[13] and the azeotropic line (filled squares)[11,13,15,17,19−22] The curves represent the theoretical predictions of the gas−liquid critical line (dashed curve), the gas−liquid coexistence (thin solid curve), and the azeotropic line (dashed−dotted curve).

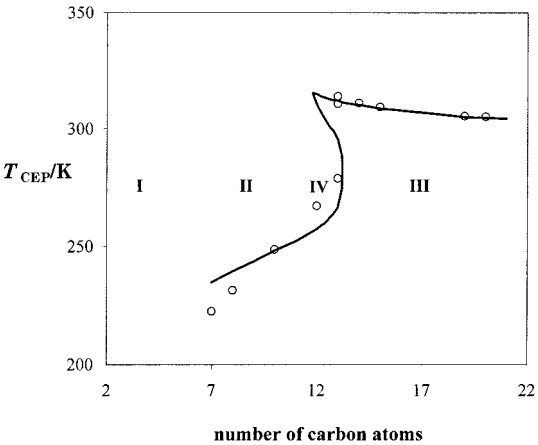

Figure 9. Critical end-point (CEP) temperatures for mixtures CO_2 + *n*-alkane compared with the SAFT-VR predictions for increasing *n*-alkane chain length. The open circles correspond to the experimental data,[56] and the curve to the predictions using the SAFT-VR approach. The types of fluid phase behavior, which can be determined from inspection of the CEPs, are also indicated. See also Table 2 for further details.

from ethane to *n*-hexadecane), it is useful to obtain a different set of parameters in order to obtain quantitative agreement with the experimental data in the case of the mixtures with shorter *n*-alkanes. Hence, ξ is readjusted to predict the locus of the maximum pressure in the gas−liquid critical line of the CO_2 + *n*-butane binary mixture (349.3 K and 8.142 MPa);[24,25] the optimized value is $\xi = 0.94$. Note that the binary interaction parameter that determines the unlike range of the square-well interactions, γ, has the same value for all of the carbon dioxide + *n*-alkane binary mixtures considered ($\gamma = 0.989$). This set of parameters is found to give an excellent representation of the phase behavior, both in terms of critical curves and coexistence compositions for mixtures of carbon dioxide + ethane, + propane, + *n*-butane, and + *n*-pentane. The SAFT-VR calculations using $\xi = 0.94$ and $\gamma = 0.989$ for the CO_2 + ethane system can be seen in Figures 7 and 8. The calculated minimum temperature of the gas−liquid critical line, 291.04 K and 5.93 MPa, is in excellent agreement with experimental data (291.04 K and 5.79 MPa).[23] Furthermore, the coexistence compositions at several constant temperatures have also been obtained using the same set of unlike parameters ($\xi = 0.94$ and $\gamma = 0.989$; see Figure 8).

It is known that CO_2 + *n*-alkane mixtures exhibit type I phase behavior for *n*-alkanes from methane up to *n*-hexane. It is important to note, however, that in the carbon dioxide + *n*-hexane mixture a metastable liquid−liquid immiscibility region below the SSLV quadruple point has been measured experimentally (this is a clear example of how immiscibility gaps are usually preempted by the appearance of the solid phases). Although the SAFT-VR approach provides an excellent description of the phase behavior of shorter *n*-alkanes with carbon dioxide, it also predicts the existence of liquid−liquid immiscibility (characteristics of type II class) in all systems, provided the temperature is low enough; this is direct consequence of the fact the SAFT approach is a fluid-phase equation of state and does not incorporate the characteristics of the solid phases.

In Figure 9, we summarize the global phase diagram for mixtures carbon dioxide + *n*-alkanes as obtained using the SAFT-VR approach with a unique set of unlike transferable parameters and compared to experimental data. The transitions in the types of phase behavior are best seen in terms of the critical end points of the mixtures. The CEPs delimit the regions of three-phase coexistence and, together with this, the extent of liquid−liquid immiscibility. Mixtures of type I phase behavior present no CEPs (these are preempted by the appearance of the solid phases), systems of type II present one CEP at low temperatures, whereas mixtures of type III present one CEP close to, and above, the critical point of the more volatile component (in our case CO_2). The transition from type II to type III occurs via type IV phase behavior, which presents three CEPs limiting the two three-phase lines. The experimental CEPs

for CO_2 + *n*-alkane mixtures from *n*-heptane to *n*-eicosane[56] are presented. As mentioned, we have used a unique set of unlike parameters $\xi = 0.88$ and $\gamma = 0.989$ (those obtained to ensure that the CO_2 + *n*-tridecane binary mixture exhibits type IV phase behavior) to calculate and predict the phase behavior of all of the mixtures. It should be noted that the limits of immiscibility (i.e., the types of phase behavior) play a crucial role in determining the conditions for supercritical extraction in carbon dioxide. As can be seen in the figure, the theoretical curves presented are not as smooth as might be desirable, and this is due to the numerical technique used to obtained them. Higher precision in the calculation together with a fine grid of intermediate mixtures would improve these results.

The global phase diagram shown in Figure 9 describing the continuous transitions in types of phase behavior for CO_2 + *n*-alkane binary mixtures is similar to those presented previously by Scott and van Konynenburg[8,9] and Scott and co-workers.[151−155] In the first case, the critical end-point properties are plotted against the dispersive energy ratio (a_{22}/a_{11}) parameter of the van der Waals equation of state which accounts for the asymmetry between the components of the mixture (see Figure 3 of the work of Scott and Konynenbrug[8]). In the second case, a similar plot is used to study the tricritical behavior of pseudobinary mixtures of *n*-alkanes. This particular type of system has been also studied by Blas and Vega[121,122] using the *Soft*-SAFT equation of state. All of these examples, as well as the current work, clearly show how the equations of state are able to predict the continuity in fluid phase behavior observed in experimental binary mixtures.

4. Conclusions

A global view of the fluid phase behavior of carbon dioxide mixtures with *n*-alkanes is given using the SAFT-VR approach and experimental data taken from the literature. The phase behavior of these mixtures is of interest in the context of supercritical extraction. The *n*-alkanes, and most organic molecules, present rather limited solubility in carbon dioxide, an important drawback in the purification process. In the classification of Scott and van Konynenburg for binary mixtures, such limited miscibility of the liquid phases corresponds to the so-called types II (for shorter, more soluble alkanes) and III (for the longer, more insoluble alkanes). We are able to predict these transitions in the type of phase behavior for a series of *n*-alkanes from ethane to *n*-hexadecane using a unique set of transferable parameters. The molecular parameters of carbon dioxide are determined by fittings to the experimental vapor pressure and saturated liquid density, and the parameters corresponding to the *n*-alkanes are taken from a previous work.[101] Both sets of parameters are rescaled to the experimental critical points of the pure components as our main interest is on the critical and supercritical regions. The unlike interaction and range parameters are determined ensuring that the CO_2 + *n*-tridecane exhibits type IV phase behavior (the transition between types II and III). This unique set of binary interaction parameters can be used in the SAFT-VR approach to predict the transitions in the type of phase behavior observed when the molecular weight of the alkane is varied. The global phase diagram of CO_2 + *n*-alkane mixtures is presented in terms of the critical end points for the mixtures of CO_2 + *n*-heptane up to *n*-eicosane. Equations of state can offer a global and continuous picture of the fluid phase behavior of complex mixtures. In the context of carbon dioxide mixtures, this view is of particular applied interest. We plan to extend this work by examining solubility of polymer molecules in supercritical carbon dioxide, incorporating in the approach different CO_2-phobic and CO_2-philic groups.

Acknowledgment. A.G. thanks the Engineering and Physical Sciences Research Council (EPSRC) for the award of an Advanced Research Fellowship, and F.J.B. thanks the Oil Extraction program of the EPSRC for a research fellowship (GR/N20317). This work was also supported by a research project from VII Plan Propio de Investigación de la Universidad de Huelva. This financial support is gratefully acknowledged.

References and Notes

(1) Vargaftik, N. B. *Table on Thermophysical properties of liquids and gases*; Hemisphere Publishing: New York, 1975.
(2) Rowlinson, J. S.; Swinton, F. L. *Liquids and liquid mixtures*, 3rd ed.; Butterworth Scientific: London, 1982.
(3) DeSimone, J. M.; Guan, Z.; Elsbernd, C. S. *Science* **1992**, *257*, 945.
(4) Yazdi, A. V.; Beckman, E. J. *Ind. Eng. Chem. Res.* **1996**, *35*, 3644.
(5) Yazdi, A. V.; Beckman, E. J. *Ind. Eng. Chem. Res.* **1997**, *36*, 2368.
(6) Diep, P.; Jordan, K. D.; Johnson, J. K.; Beckman, E. J. *J. Phys. Chem. A* **1998**, *102*, 2231.
(7) Schneider, G. M. *J. Suprercrit. Fluids* **1998**, *13*, 5.
(8) Scott, R. L.; van Konynenburg, P. H. *Discuss. Faraday Soc.* **1970**, *49*, 87.
(9) van Konynenburg, P. H.; Scott, R. L. *Philos. Trans. R. Soc. London A* **1980**, *298*, 495.
(10) Kuenen, J. P. *Philos. Mag.* **1897**, *44*, 175.
(11) Kuenen, J. P. *Z. Phys. Chem.* **1897**, *24*, 667.
(12) Kuenen, J. P.; Robson, W. G. *Philos. Mag.* **1902**, *4*, 116.
(13) Fredeuslund, A.; Mollerup, J. *J. Chem. Soc., Faraday Trans. 1* **1974**, *70*, 1653.
(14) Mollerup, J. J. *J. Chem. Soc., Faraday Trans. 1* **1975**, *71*, 2351.
(15) Wei, M. S.-W.; Brown, T. S.; Kidnay, A. J.; Sloan, E. D. *J. Chem. Eng. Data* **1995**, *40*, 726.
(16) Brown, T. S.; Kidnay, A. J.; Sloan, E. D. *Fluid Phase Equilib.* **1988**, *40*, 169.
(17) Clark, A. Q.; Stead, K. *J. Chem. Thermodyn.* **1988**, *20*, 413.
(18) Ohgaki, K.; Katayama, T. *Fluid Phase Equilib.* **1977**, *1*, 27.
(19) Khazanova, N. E.; Lesnevskaya, L. S.; Zakharova, A. V. *Khim. Promst.* **1966**, *44*, 364.
(20) Davalos, J.; Anderson, W. R.; Phelps, R. E.; Kidnay, A. J. *J. Chem. Eng. Data* **1976**, *21*, 81.
(21) Khazanova, N. E.; Lesnevskaya, L. S. *Zh. Fiz. Khim.* **1967**, *41*, 2373.
(22) Rowlinson, J. S.; Sutton, J. R. *Proc. R. Soc. London Ser. A* **1955**, *229*, 396.
(23) Horstmann, S.; Fischer, K.; Gmehling, J.; Kolář, P. *J. Chem. Thermodyn.* **2000**, *32*, 451.
(24) Poettmann, F. H.; Katz, D. L. *Ind. Eng. Chem.* **1945**, *37*, 847.
(25) Olds, R. H.; Reamer, H. H.; Sage, B. H.; Lacey, W. N. *Ind. Eng. Chem.* **1949**, *41*, 475.
(26) Reamer, H. H.; Sage, B. H.; Lacey, W. N. *Ind. Eng. Chem.* **1951**, *43*, 2515.
(27) Nagahama, K.; Konishi, H.; Hoshino, D.; Hirata, M. *J. Chem. Eng. Jpn.* **1974**, *7*, 323.
(28) Haseldon, G. C.; Newitt, D. M.; Shah, S. M. *Proc. R. Soc. A* **1951**, *209*, 1.
(29) Besserer, G. J.; Robinson, D. B. *J. Chem. Eng. Data* **1973**, *18*, 298.
(30) Roof, J. G.; Baron, J. D. *J. Chem. Eng. Data* **1967**, *12*, 292.
(31) Bushner, E. H. *Z. Phys. Chem.* **1906**, *54*, 665.
(32) Van Poolen, L. J.; Holcomb, C. D. *Fluid Phase Equilib.* **1999**, *165*, 157.
(33) Stewart, W. C.; Nielsen, R. F. *Prod. Mon.* **1954**, *18*, 27.
(34) Reamer, H. H.; Sage, B. H. *J. Chem. Eng. Data* **1963**, *8*, 508.
(35) Li, Y. H.; Dillard, K. H.; Robinson, R. L. *J. Chem. Eng. Data* **1981**, *26*, 53.
(36) Ohgaki, K.; Katayama, T. *J. Chem. Eng. Data* **1976**, *21*, 53.
(37) Kalra, H.; Kubota, H.; Robinson, R. L.; Ng, H.-J. *J. Chem. Eng. Data* **1978**, *23*, 317.
(38) Sebastian, H. M.; Simnick, J. J.; Liu, H. M.; Chao, K. C. *J. Chem. Eng. Data* **1980**, *25*, 138.
(39) Huie, N. C.; Luks, K. D.; Kohn, J. P. *J. Chem. Eng. Data* **1973**, *18*, 311.
(40) Fall, D. J.; Luks, K. D. *J. Chem. Eng. Data* **1984**, *29*, 413.

(41) Gasem, K. A. M.; Robinson, R. L. *J. Chem. Eng. Data* **1985**, *30*, 53.
(42) Sato, Y.; Tagashira, Y.; Maruyama, D.; Takishima, S.; Masuoka, H. *Fluid Phase Equilib.* **1998**, *147*, 181.
(43) Schneider, G. M. *Ber. Bunsen-Ges. Phys. Chem.* **1966**, *70*, 10.
(44) Schneider, G. M. *Ber. Bunsen-Ges. Phys. Chem.* **1966**, *70*, 497.
(45) Schneider, G. M.; Alwani, Z.; Heim, W.; Horvath, E.; Franck, E. U. *Chem. Eng. Technol.* **1967**, *39*, 649.
(46) Schneider, G. M. *Chem. Eng. Prog. Symp. Ser.* **1968**, *64*, 9.
(47) Kulkarni, A. A.; Zorah, B. Y.; Luks, K. D.; Kohn, J. P. *J. Chem. Eng. Data* **1974**, *19*, 92.
(48) van der Steen, J.; de Loos, Th. W.; de Swaan Arons, J. *Fluid Phase Equilib.* **1989**, *51*, 353.
(49) Hottovy, J. D.; Luks, K. D.; Kohn, J. P. *J. Chem. Eng. Data* **1981**, *26*, 256.
(50) Enick, R.; Holder, G. D.; Morsi, B. I. *Fluid Phase Equilib.* **1985**, *22*, 209.
(51) Fall, D. J.; Luks, K. D. *J. Chem. Eng. Data* **1985**, *30*, 276.
(52) Jensen, R. H. Ph.D. Thesis, University of Kansas, Lawrence, Kansas, 1969.
(53) Im, U. K. Ph.D. Thesis, University of Kansas, Lawrence, Kansas, 1970.
(54) Francis, A. W. *Ind. Eng. Chem.* **1944**, *36*, 764.
(55) Im, U. K.; Kurata, F. *J. Chem. Eng. Data* **1971**, *16*, 412.
(56) Miller, M. M.; Luks, K. D. *Fluid Phase Equilib.* **1989**, *44*, 295.
(57) Hottovy, J. D.; Kohn, J. P.; Luks, K. D. *J. Chem. Eng. Data* **1982**, *27*, 298.
(58) Fall, D. J.; Fall, J. L.; Luks, K. D. *J. Chem. Eng. Data* **1985**, *30*, 82.
(59) Brunner, E. *J. Chem. Thermodyn.* **1990**, *22*, 335.
(60) Prausnitz, J. M.; Lichtentaler, R. N.; Gomes de Azevedo, E. *Molecular thermodynamics of fluid phase equilibria*, 2nd ed.; Prentice Hall Inc.: Englewood Cliffs, New Jersey, 1986.
(61) Peng, D.-Y.; Robinson, D. B. *Ind. Eng. Chem. Fundam.* **1976**, *15*, 59.
(62) Soave, G. *Chem. Eng. Sci.* **1972**, *27*, 1197.
(63) Coutinho, J. A. P.; Kontogeorgis, G. M.; Stenby, E. H. *Fluid Phase Equilib.* **1994**, *102*, 31.
(64) Beret, S.; Prausnitz, J. M. *AIChE J.* **1975**, *21*, 1123.
(65) Kim, C.-H.; Vimalchand, P.; Donohue, M. D.; Sandler, S. I. *AIChE J.* **1986**, *32*, 1726.
(66) Lee, K. H.; Lombardo, M.; Sandler, S. I. *Fluid Phase Equilib.* **1985**, *21*, 177.
(67) Gubbins, K. E.; Twu, C. H. *Chem. Eng. Sci.* **1978**, *33*, 863.
(68) Twu, C. H.; Gubbins, K. E. *Chem. Eng. Sci.* **1978**, *33*, 879.
(69) Stell, G.; Rasaiah, J. C.; Narang, H. *Mol. Phys.* **1974**, *27*, 1393.
(70) Ikonomou, G. D.; Donohue, M. D. *AICHE J.* **1986**, *32*, 1716.
(71) Benavides, A. L.; Guevara, Y.; Del Río, F. *Physica A* **1994**, *202*, 420.
(72) Del Río, F.; Benavides, A. L. *Physica A* **1995**, *215*, 10.
(73) Guevara, Y.; Benavides, A. L.; Del Río, F. *Mol. Phys.* **1996**, *89*, 1277.
(74) Benavides, A. L.; Guevara, Y.; Estrada-Alexanders, A. F. *J. Chem. Thermodyn.* **2000**, *32*, 945.
(75) Chapman, W. G.; Gubbins, K. E.; Jackson G.; Radosz, M. *Fluid Phase Equilib.* **1989**, *52*, 31.
(76) Chapman, W. G.; Gubbins, K. E.; Jackson, G.; Radosz, M. *Ind. Eng. Chem. Res.* **1990**, *29*, 1709.
(77) Wertheim, M. S. *J. Stat. Phys.* **1984**, *35*, 19.
(78) Wertheim, M. S. *J. Stat. Phys.* **1984**, *35*, 35.
(79) Wertheim, M. S. *J. Stat. Phys.* **1986**, *42*, 459.
(80) Wertheim, M. S. *J. Stat. Phys.* **1986**, *42*, 477.
(81) Jackson, G.; Chapman, W. G.; Gubbins, K. E. *Mol. Phys.* **1988**, *65*, 1.
(82) Chapman, W. G.; Jackson, G.; Gubbins, K. E. *Mol. Phys.* **1988**, *65*, 1057.
(83) Wertheim, M. S. *J. Chem. Phys.* **1986**, *85*, 2929.
(84) Wertheim, M. S. *J. Chem. Phys.* **1987**, *87*, 7323.
(85) Huang, S. H.; Radosz, M. *Ind. Eng. Chem. Res.* **1990**, *29*, 2284.
(86) Huang, S. H.; Radosz, M. *Ind. Eng. Chem. Res.* **1991**, *30*, 1994.
(87) Müller, E. A.; Gubbins, K. E. *Equations of state for fluids And fluid mixtures*; Elsevier: Amsterdam, The Netherlands, 2000; Chapter 12.
(88) Müller, E. A.; Gubbins, K. E. *Ind. Eng. Chem. Res.* **2001**, *40*, 2193.
(89) Galindo, A.; Whitehead, P. J.; Jackson, G.; Burgess, A. N. *J. Phys. Chem.* **1996**, *100*, 6781.
(90) Galindo, A.; Whitehead, P. J.; Jackson, G.; Burgess, A. N. *J. Phys. Chem. B* **1997**, *101*, 2082.
(91) García-Lisbona, M. N.; Galindo, A.; Jackson, G.; Burgess, A. N. *Mol. Phys.* **1998**, *93*, 57.
(92) García-Lisbona, M. N.; Galindo, A.; Jackson, G.; Burgess, A. N. *J. Am. Chem. Soc.* **1998**, *120*, 4191.
(93) Blas, F. J.; Vega, L. F. *J. Chem. Phys.* **2001**, *115*, 3906.
(94) Gil-Villegas, A.; Galindo, A.; Whitehead, P. J.; Mills, S. J.; Jackson, G.; Burgess, A. N. *J. Chem. Phys.* **1997**, *106*, 4168.
(95) Galindo, A.; Davies, L. A.; Gil-Villegas, A.; Jackson, G. *Mol. Phys.* **1998**, *93*, 241.
(96) Davies, L. A.; Gil-Villegas, A.; Jackson, G. *Int. J. Thermophys.* **1998**, *19*, 675.
(97) Davies, L. A.; Gil-Villegas, A.; Jackson, G. *J. Chem. Phys.* **1999**, *111*, 8659.
(98) McCabe, C.; Galindo, A.; Gil-Villegas, A.; Jackson, G. *Int. J. Thermophys.* **1998**, *19*, 1511.
(99) McCabe, C.; Gil-Villegas, A.; Jackson, G. *J. Phys. Chem. B* **1998**, *102*, 4183.
(100) McCabe, C.; Galindo, A.; Gil-Villegas, A.; Jackson, G. *J. Phys. Chem. B* **1998**, *102*, 8060.
(101) McCabe, C.; Jackson, G. *Phys. Chem. Chem. Phys.* **1999**, *1*, 2057.
(102) Galindo, A.; Gil-Villegas, A.; Whitehead, P. J.; Jackson, G. *J. Phys. Chem. B* **1998**, *102*, 7632.
(103) Galindo, A.; Florusse, L. J.; Peters, C. J. *Fluid Phase Equilib.* **1999**, *160*, 123.
(104) Galindo, A.; Gil-Villegas, A.; Jackson, G.; Burgess, A. N. *J. Phys. Chem. B* **1999**, *103*, 10272.
(105) Gil-Villegas, A.; Galindo, A.; Jackson, G. *Mol. Phys.* **2001**, *99*, 531.
(106) McCabe, C.; Galindo, A.; Garcia-Lisbona, M. N.; Jackson, G. *Ind. Eng. Chem. Res.* **2001**, *40*, 3835.
(107) Gross, J.; Sadowski, G. *Fluid Phase Equilib.* **2000**, *168*, 183.
(108) Gross, J.; Sadowski, G. *Ind. Eng. Chem. Res.* **2001**, *40*, 1244.
(109) Chapman, W. G. *J. Chem. Phys.* **1990**, *93*, 4299.
(110) Ghonasgi, D.; Chapman, W. G. *Mol. Phys.* **1993**, *80*, 161.
(111) Johnson, J. K.; Gubbins, K. E. *Mol. Phys.* **1992**, *77*, 1033.
(112) Ghonasgi, D.; Llano-Restrepo, M.; Chapman, W. G. *J. Chem. Phys.* **1993**, *98*, 5662.
(113) Ghonasgi, D.; Chapman, W. G. *AIChE J.* **1994**, *40*, 878.
(114) Johnson, J. K.; Müller, E. A.; Gubbins, K. E. *J. Phys. Chem.* **1994**, *98*, 6413.
(115) Müller, E. A.; Gubbins, K. E. *Ind. Eng. Chem. Res.* **1995**, *34*, 3662.
(116) Kraska, T.; Gubbins, K. E. *Ind. Eng. Chem. Res.* **1996**, *35*, 4727.
(117) Kraska, T.; Gubbins, K. E. *Ind. Eng. Chem. Res.* **1996**, *35*, 4738.
(118) Jog, P. K.; Chapman, W. G. *Mol. Phys.* **1999**, *97*, 307.
(119) Blas, F. J.; Vega, L. F. *Mol. Phys.* **1997**, *92*, 135.
(120) Blas, F. J.; Vega, L. F. *Ind. Eng. Chem. Res.* **1998**, *37*, 660.
(121) Blas, F. J.; Vega, L. F. *J. Chem. Phys.* **1998**, *109*, 7405.
(122) Vega, L. F.; Blas, F. J. *Fluid Phase Equilib.* **2000**, *171*, 91.
(123) Johnson, J. K. *J. Chem. Phys.* **1996**, *104*, 1729.
(124) Blas, F. J.; Vega, L. F. *J. Chem. Phys.* **2001**, *115*, 4355.
(125) Pàmies, J. C.; Vega, L. F. *Ind. Eng. Chem. Res.* **2001**, *40*, 2532.
(126) Vega, C.; MacDowell, L. *J. Chem. Phys.* **2001**, *114*, 10411.
(127) Gloor, G. J.; Blas, F. J.; Martín del Río, E.; de Miguel, E.; Jackson, G. *Fluid Phase Equilib.* **2002**, *194*−*197*, 521.
(128) Blas, F. J.; Martín del Río, E.; de Miguel, E.; Jackson, G. *Mol. Phys.* **2001**, *99*, 1851.
(129) Filipe, E. J. M.; Gomes de Azebedo, E. J. S.; Martins, L. F. G.; Soares, V. A. M.; Calado, J. C. G.; McCabe, C.; Jackson, G. *J. Phys. Chem. B* **2000**, *104*, 1315.
(130) Filipe, E. J. M.; Martins, L. F. G.; Calado, J. C. G.; McCabe, C.; Jackson, G. *J. Phys. Chem. B* **2000**, *104*, 1322.
(131) MacDowell, L. G.; Vega, C.; López-Rodríguez, A. *J. Chem. Phys.* **1999**, *111*, 3192.
(132) Blas, F. J. *J. Phys. Chem. B* **2000**, *104*, 9239.
(133) Passarello, J. P.; Benzaghou, S.; Tobaly, P. *Ind. Eng. Chem. Res.* **2000**, *39*, 2578.
(134) Luna-Barcenas, G.; Mawson, S.; Takishima, S.; DeSimone, J. M.; Sanchez, I. C.; Johnston, K. P. *Fluid Phase Equilib.* **1998**, *146*, 325.
(135) Wiesmet, V.; Weidner, E.; Behme, S.; Sadowski, G.; Arlt, M. *J. Supercrit. Fluids* **2000**, *17*, 1.
(136) Byun, H. S.; Kim, K.; McHugh, M. A. *Ind. Eng. Chem. Res.* **2000**, *39*, 4580.
(137) Potoff, J. J.; Errington, J. R.; Panagiotopoulos, A. Z. *Mol. Phys.* **1999**, *97*, 1073.
(138) Potoff, J. J.; Siepmann, J. I. *AIChE J.* **2001**, *47*, 1676.
(139) Cui, S. T.; Cochran, H. D.; Cummings, P. T. *J. Phys. Chem. B* **1999**, *103*, 4485.
(140) Blas, F. J.; Galindo, A. *Fluid Phase Equilib.* **2002**, *194*−*197*, 501.
(141) Jackson, G.; Gubbins, K. E. *Pure Appl. Chem.* **1989**, *61*, 1021.
(142) Hansen, J. P.; McDonald, I. R. *Theory of Simple Liquids*, 2nd ed.; Academic Press: New York, 1986.
(143) Barker, J. A.; Henderson, D. *J. Chem. Phys.* **1967**, *47*, 2856.
(144) Barker, J. A.; Henderson, D. *J. Chem. Phys.* **1967**, *47*, 4714.
(145) Barker, J. A.; Henderson, D. *Rev. Mod. Phys.* **1976**, *48*, 587.
(146) Boublík, T. *J. Chem. Phys.* **1970**, *53*, 471.
(147) Mansoori, G. A.; Carnahan, N. F.; Starling, K. E.; Leland, T. W. *J. Chem. Phys.* **1971**, *54*, 1523.

(148) Carnahan, N. F.; Starling, K. E. *J. Chem. Phys.* **1969**, *51*, 635.
(149) Press, W. H.; Teukolsky, S. A.; Vetterling, W. T.; Flannery, B. P. *Numerical Recipes in Fortran*, 1st ed.; Cambridge University Press: Cambridge, U.K., 1986.
(150) Smith, B. D.; Srivastava, R. *Thermodynamic data for Pure Compounds*; Elsevier: New York, 1986.
(151) Creek, J. L.; Knobler, C. M.; Scott, R. L. *J. Chem. Phys.* **1977**, *67*, 366.
(152) Creek, J. L.; Knobler, C. M.; Scott, R. L. *J. Chem. Phys.* **1981**, *74*, 3489.
(153) Goh, M. C.; Specovius, J.; Scott, R. L.; Knobler, C. M.; *J. Chem. Phys.* **1987**, *86*, 4120.
(154) Fernandez-Fassnacht, E.; Williamson, A. G.; Sivaraman, A.; Scott, R. L.; Knobler, C. M. *J. Chem. Phys.* **1987**, *86*, 4133.
(155) Goh, M. C.; Scott, R. L.; Knobler, C. M. *J. Chem. Phys.* **1988**, *89*, 2281.